Supporting Information

Origin of the electrocatalytic oxygen reduction activity of graphene-based catalysts: a roadmap to achieve the best performance

Yan Jiao[1†], Yao Zheng[1,2†], Mietek Jaroniec[3], Shi Zhang Qiao[1*]

[1] *School of Chemical Engineering, The University of Adelaide, Adelaide, SA 5005, Australia*

[2] *Australian Institute for Bioengineering and Nanotechnology (AIBN), The University of Queensland, St Lucia, QLD 4067, Australia*

[3] *Department of Chemistry and Biochemistry, Kent State University, Kent, OH 44242, United States*

† These authors contributed equally to this work.

This PDF file includes:

Part I: Experimental Section

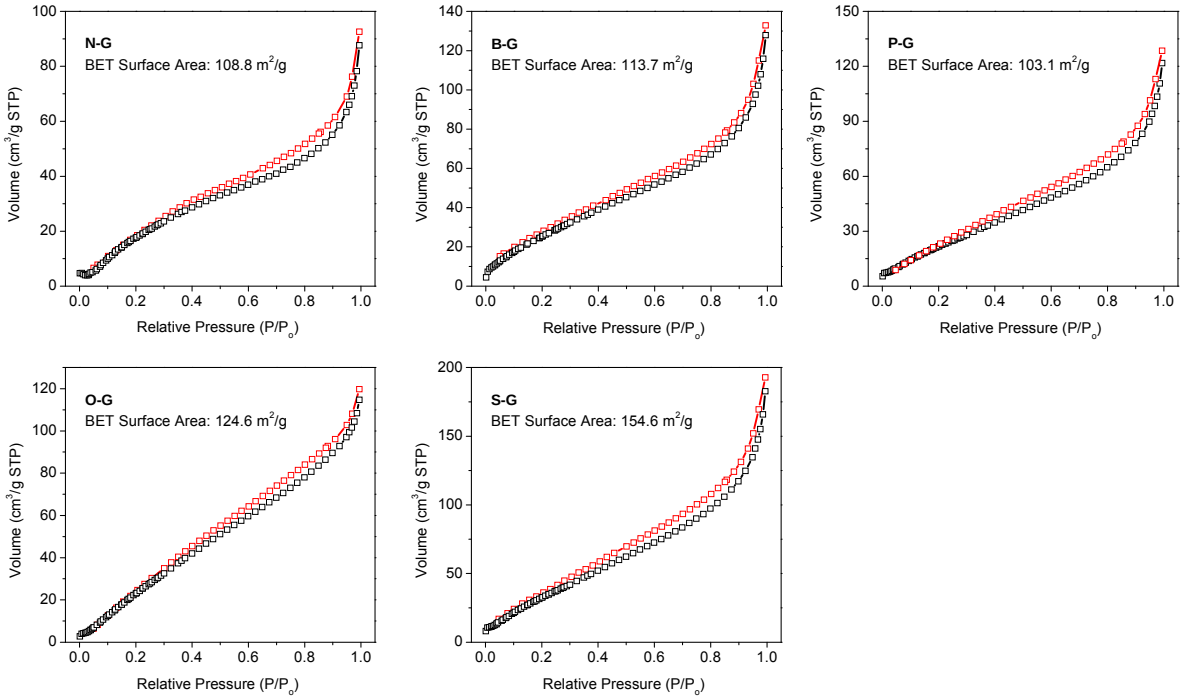

Figure S1 Nitrogen adsorption isotherms and BET surface areas for various chemically synthesized doped graphenes.

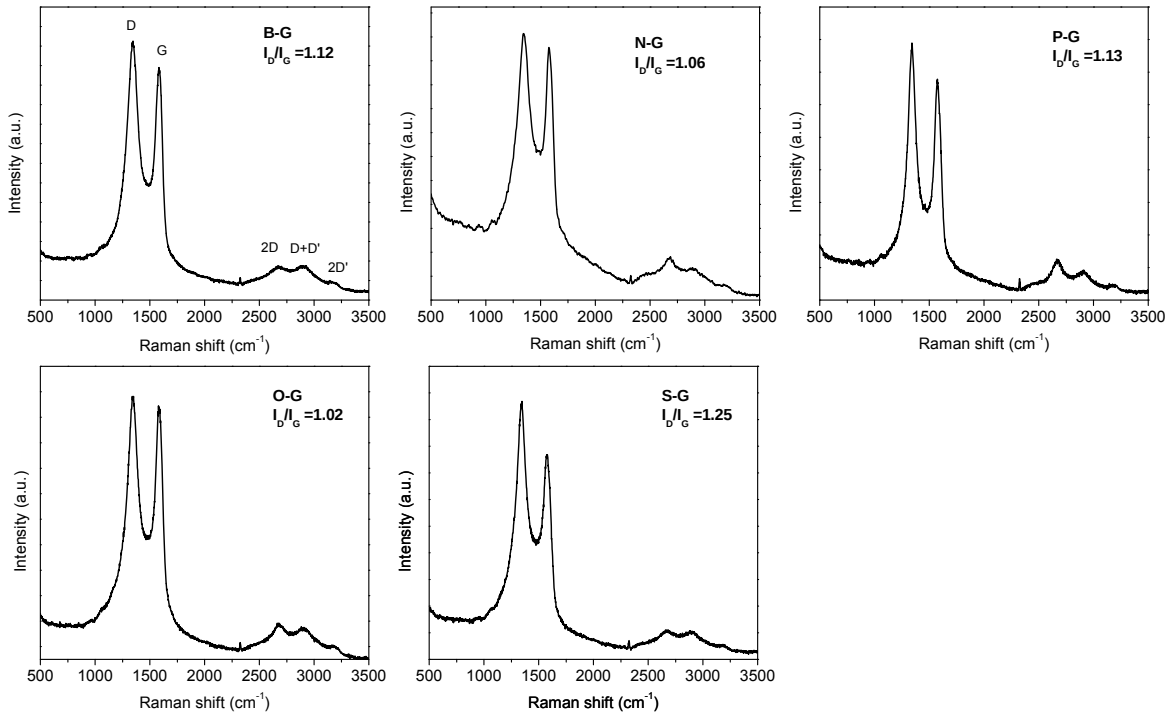

Figure S2 Raman spectra and I_D/I_G ratios for various chemically synthesized doped graphenes.

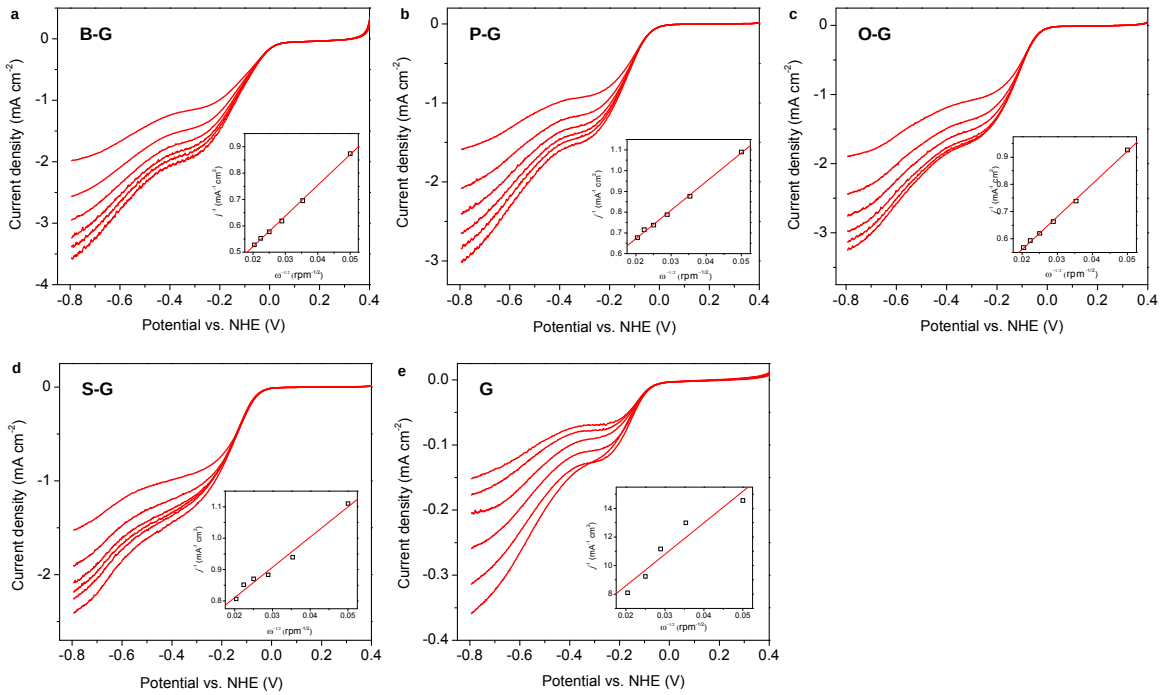

Figure S3 The LSV curves obtained at RDE with different rotating rates (400 to 2,400 rpm) in O_2-saturated 0.1M KOH solution and the corresponding K-L plot (inset) on -0.3 V vs. NHE on the basis of RDE data.

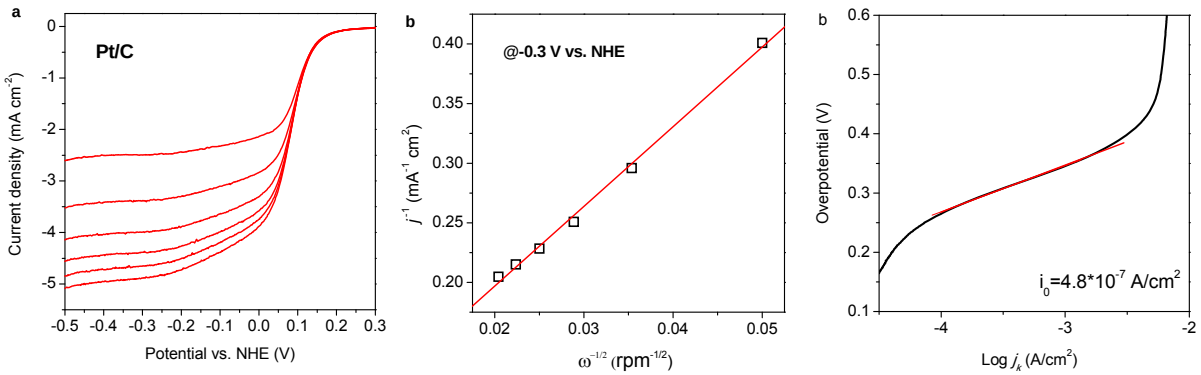

Figure S4 (**a,b)** LSV of commercial 20% Pt/C at RDE with different rotating rates (400 to 2,400 rpm) in O_2-saturated 0.1M KOH solution and the corresponding K-L plot (inset) on -0.3 V vs. NHE on the basis of RDE data. **(c)** Tafel plot and calculated exchange current density of Pt/C.

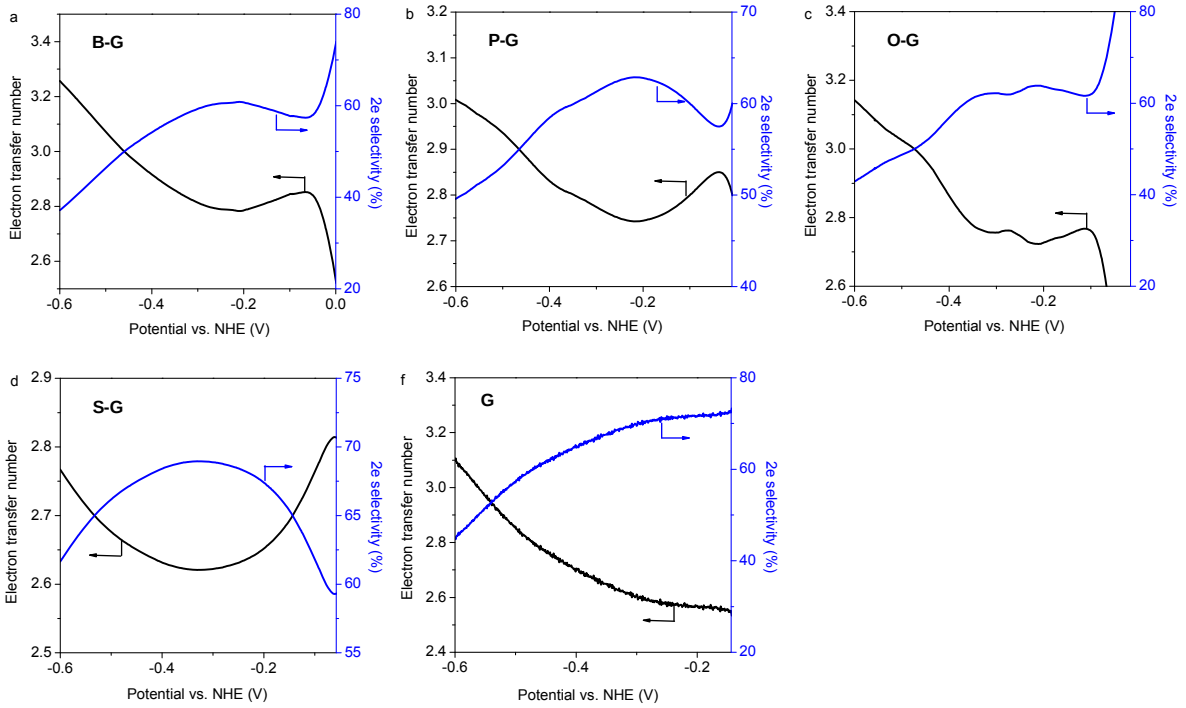

Figure S5 Electron transfer number (black) and the corresponding $2e^-$ ORR pathway selectivity (blue) for various doped graphene electrocatalysts.

Table S1 ORR exchange current density for different heteroatom doped graphenes.

	N-G	B-G	P-G	O-G	S-G	G
$U^{on\text{-}set}$ (V, vs NHE)[a]	0.035	0.029	–0.011	–0.017	–0.058	–0.145
j_0 (A/cm^2)	3.0×10^{-9}	7.6×10^{-9}	7.7×10^{-11}	6.3×10^{-11}	3.5×10^{-12}	9.5×10^{-12}
J_k@-0.3 V (mA/cm^2)	–2.29	–2.38	–1.82	–2.13	–1.45	–0.29
J_k@-0.2 V (mA/cm^2)	–1.76	–1.79	–1.37	–1.66	–0.94	–0.19
J_k@-0.1 V (mA/cm^2)	–0.86	–0.84	–0.48	–0.60	–0.24	–0.04

[a] The on-set potential is defined as potential that corresponds to –0.005 mA/cm^2 current density on LSV

Part II: Computational Section

2.1 Model Building

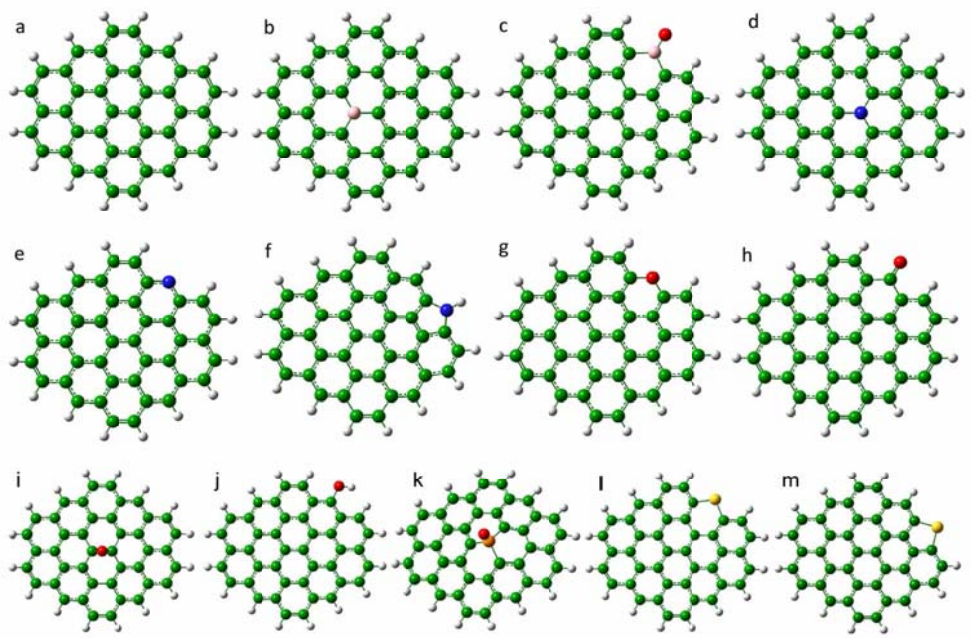

Figure S6 (a) pure graphene (G), **(b)** graphitic boron-doped graphene (gB-G), **(c)** B-2C-O type boron-doped graphene (OB-G), **(d)** graphitic N-graphene (gN-G), **(e)** pyridinic nitrogen-doped graphene (pdN-G), **(f)** pyrrolic nitrogen-doped graphene (prN-G), **(g)** pyran type oxygen-doped graphene (pyO-G), **(h)** carbonyl oxygen-doped graphene (C=O-G), **(i)** epoxy oxygen-doped graphene (epO-G), **(j)** hydroxyl type oxygen-doped graphene (C-OH-G), **(k)** phosphorus-doped graphene (P-G), **(l)** C-S-C type sulphur-doped graphene (SC6-G), **(m)** thiophen type sulphur-doped graphene (SC5-G). Green, blue, red, pink, orange, lemon, and white spheres represent carbon, nitrogen, oxygen, boron, phosphorous, sulphur, and hydrogen atoms, respectively.

2.2 Reaction Scheme and Free Energy

ORR Pathways and the Dissociative 4e⁻ Pathway

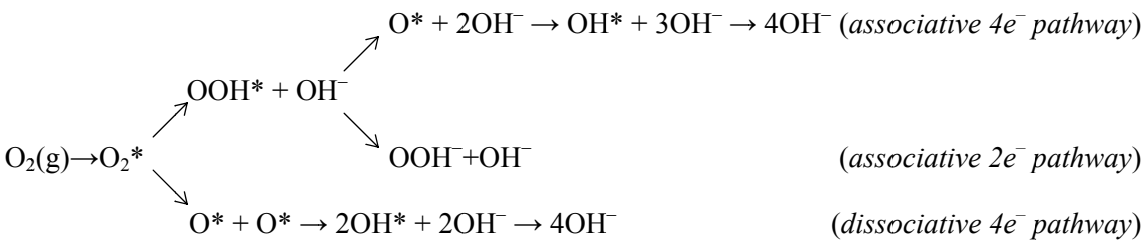

Scheme S1 Possible reaction pathways of ORR in alkaline solution.[1]

Among the pathways in Scheme S1, the $4e^-$ reduction pathway on doped graphene catalyst was selected to be the associative pathway, rather than the dissociative pathway, based on several previous studies and our own calculations. Firstly Yu *et al* proposed that dissociation pathway does not exist on graphitic nitrogen-doped graphene surface[1]. Another first principles computational work showed that the O_2 dissociation barriers on graphene and nitrogen-doped graphene are 2.39 eV and 1.20 eV, respectively; both are not surmountable at room temperature[2]. Additionally, we have examined the O_2 dissociation pathway on graphitic boron-doped graphene (gB-G) cluster as shown in Fig. S6. The energy barrier for O_2 dissociation is 2.17 eV, also suggests that the dissociative $4e^-$ pathway is not possible at room temperature. Hence, in this article only the associative $4e^-$ reduction pathway is considered.

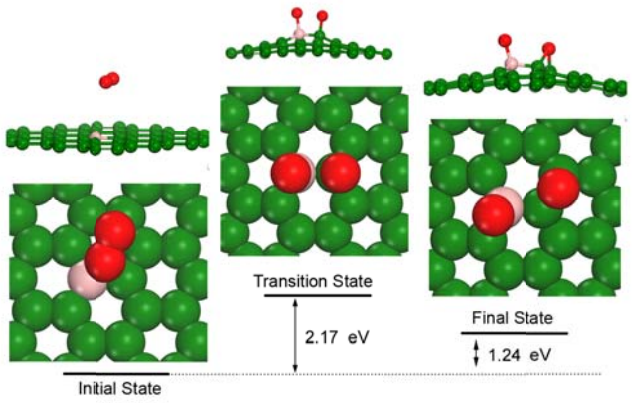

Figure S7 O_2 dissociation pathway on gB-G (structure adopted from Fig. S6b) to form two adsorbed O*. Each state includes a side view and a top view; energy levels are not drawn to scale. Green is carbon, red is oxygen, and pink is boron. Hydrogen atoms at the edge are not shown in this figure.

Free Energy Calculation

Table S2 Atomic composition and electron numbers of each state in Fig. 3a (from left to right).

State	Composition	Electrons
O_2 (reactant)	$G^a + O_2(g) + 2H_2O(l)$	$4e^-$
OOH*	$OOH@G + OH^- + H_2O(l)$	$3e^-$
O*	$O@G + 2OH^- + H_2O(l)$	$2e^-$
OH*	$OH@G + 3OH^-$	$1e^-$
OH^- (product)	$G + 4OH^-$	$0e^-$

[a]G in here refers to investigated graphene with different heteroatom doping.

Since it is difficult to obtain the exact free energy of OOH, O, and OH radicals in the electrolyte solution, the adsorption free energy ΔG_{OOH*}, ΔG_{O*}, and ΔG_{OH*}, which correspond to OOH*, O*, and OH* adsorptions on graphene cluster models are defined as follows:

$$\Delta G_{OOH*}=(G_{OOH@G}+G_{H2O(l)}) - (G_G+3G_{OH-}) \quad \text{(S1a)}$$

$$\Delta G_{O*}=(G_{O@G}+G_{H2O(l)}) - (G_G+2G_{OH-}) \quad \text{(S1b)}$$

$$\Delta G_{OH*}=(G_{OH@G}) - (G_G+G_{OH-}) \quad \text{(S1c)}$$

The free energy for each step in Eqs. 9 can be related to Eqs. S1 by:

$$G_{eq(9a:right)}(U) = G_{eq(9b:left)}(U) = \Delta G_{OOH*}(U) = \Delta G_{OOH*} - 3eU \quad \text{(S2a)}$$

$$G_{eq(9b:right)}(U) = G_{eq(9c:left)}(U) = \Delta G_{O*}(U) = \Delta G_{O*} - 2eU \quad \text{(S2b)}$$

$$G_{eq(9c:right)}(U) = G_{eq(9d:left)}(U) = \Delta G_{OH*}(U) = \Delta G_{OH*} - eU \quad \text{(S2c)}$$

At equilibrium potential $U^0 = 0.455$ *vs.* NHE, since $G_{eq(9a:left)}(U^0) = G_{eq(9d:right)}(U^0) = 0$, the free energy change of the first step and the last step could be obtained from OOH* and OH* adsorption free energies:

$$\Delta G_{eq(9a)}(U^0) = \Delta G_{OOH*} - 3eU^0 \quad \text{(S3a)}$$

$$\Delta G_{eq(9d)}(U^0) = -\Delta G_{OH*} + eU^0 \quad \text{(S3b)}$$

For X-graphene, since $\Delta G_{eq(9a)}(U^0) = \Delta G_{eq(9d)}(U^0)$, then we have

$$\Delta G_{eq(9a)}(U^0) = 0.35 \text{ eV} \quad \text{(S4a)}$$

$$\Delta G_{eq(9b)}(U^0) = -0.13 \text{ eV} \quad \text{(S4b)}$$

$$\Delta G_{eq(9c)}(U^0) = -0.57 \text{ eV} \quad \text{(S4c)}$$

$$\Delta G_{eq(9d)}(U^0) = 0.35 \text{ eV} \quad \text{(S4d)}$$

$$\Delta G^{X\text{-}G}{}_{OOH*} = 1.72 \text{ eV} \quad \text{(S4e)}$$

$$\Delta G^{X\text{-}G}{}_{OH*} = 0.10 \text{ eV} \quad \text{(S4f)}$$

2.3 Exchange Current density

According to reference [3], the exchange current density for a certain electrocatalytic process can be theoretically calculated as follows:

$$j_0 = nFk^0 C_O^{1-\alpha} C_R^{\alpha} \quad \text{(S5)}$$

where n is the electron transfer number, F is the Faraday constant, k^0 is the standard rate constant, α is the transfer coefficient (a measure of the symmetry of the potential energy surface, ranging from 0 to 1), C_O is the surface concentration of oxidant O and C_R is the surface concentration of reductant R in the reaction $O + 4e^- \rightarrow R$. Simultaneously, the bulk concentrations (adjacent to the reacting surface) of C_O^* and C_R^* can be related to K at the equilibrium :

$$K = \frac{C_R}{C_O} = \frac{C_R^*}{C_O^*} = \exp[-\frac{1}{k_B T}(\Delta G_{\max}(U^0))] \quad \text{(S6)}$$

where $\Delta G_{max}(U^0)$ is the maximum value taken from $\Delta G_{eq(9a)}(U^0)$, $\Delta G_{eq(9b)}(U^0)$, $\Delta G_{eq(9c)}(U^0)$, and $\Delta G_{eq(9d)}(U^0)$, hence:

$$\Delta G_{\max}(U^0) = \begin{cases} \Delta G_{eq(9d)}(U^0) & \Delta G_{eq(9a)}(U^0) < 0.35eV \\ \Delta G_{eq(9a)}(U^0) & \Delta G_{eq(9a)}(U^0) \geq 0.35eV \end{cases} \quad \text{(S7)}$$

in which $\Delta G_{eq(9d)}(U^0) = -0.977\Delta G_{eq(9a)}(U^0) + 0.696eV$. The coverage θ for reductant R can be expressed by:

$$\theta = \frac{C_R}{C_{total}} = \frac{K}{1+K} \quad \text{(S8)}$$

where C_{total} is the sum of C_o and C_R, *i.e.* the total number of active sites. Therefore, the exchange current density can be calculated as follows:

$$j_0 = nFk^0 C_{total}[(1-\theta)^{1-\alpha}\theta^{\alpha}] \quad \text{(S9)}$$

(equation 10 in the paper), where the pre-factor $j_0 = nFk^0 C_{total}$ could be obtained by fitting the experimental data of the exchange current densities. Different α values correspond to

different pre-factors: for α=1, j_0=5.76×10^{4}A/ cm^2; for α=0.5, j_0=1.92×10^{-3}A/cm^2 as shown in Figure S8. Our observation indicates that α=0.5 assures the best representation of the measured exchange current densities, which means the reactant and product states possess a symmetric parabolic potential surface.

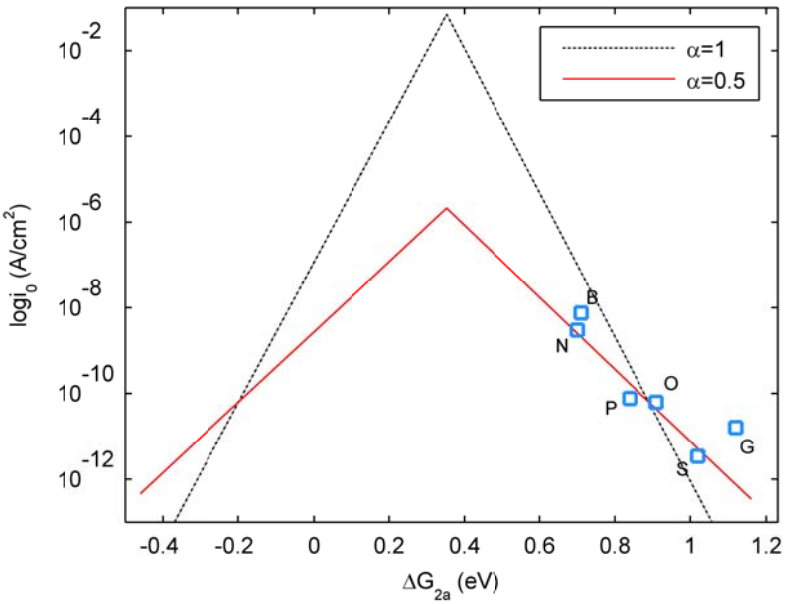

Figure S8 Volcano plot of the ORR activity represented by exchange current density for the investigated non-metallic heteroatoms doped graphene.

2.4 Reaction Pathways

Pure Graphene

For pure graphene model (Fig. S6a), two carbons (at the middle and edge of graphene the basal plane, named as G-M and G-E, respectively) were investigated upon their ability to be the active centre for ORR. Among two the G-E atom is more active for ORR due to its lower overall reaction barriers at U^0 (Fig. 9a), while the pathway on G-M is featured by two unsurmountable reaction barriers, which is consistent with earlier experimental research[4]. The inactivity of carbons far from graphene edge might be attributed to that they are all saturated by sp^2 bonding and the evenly distributed π bonding over the plane.

For G-E model, OOH*, O*, and OH* can chemisorb on G-E atom (Fig. S9b-d), while for G-M model, the optimized configurations show that OOH and OH are not bonding to the graphene surface (Fig. S9e-g).

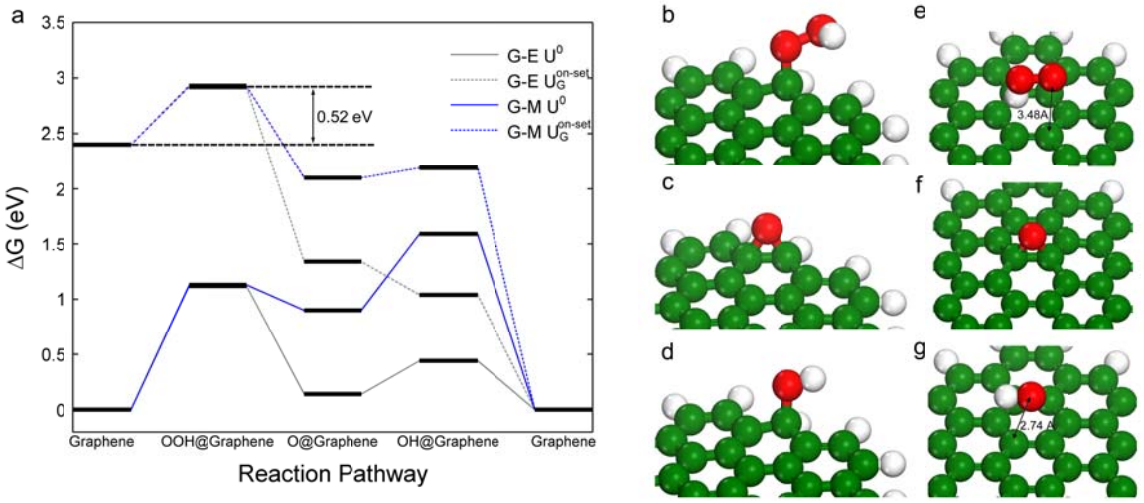

Figure S9 (a) Free energy diagram at U^0 (solid lines) and experimentally observed on-set potential $U_G^{on\text{-}set}$ = –0.145 *vs.* NHE (dash lines) for G-E (grey) and G-M (blue). (**b**-**d**) Reaction intermediates on G-E and (**e**-**g**) G-M. Green is carbon, red is oxygen, and white is hydrogen.

Boron-Doped Graphene (B-G)

Two doping models were investigated for B-G, in which gB-G (Fig. S6b) is more active than OB-G (Fig. S6c) for ORR due to its lower overall reaction barriers at U^0 (Fig. S10a). Under the experimentally observed activation electrode potential $U_B^{on\text{-}set}$=0.035 V, energy barrier for gB-G reduces to 0.29 eV.

For gB-G model, two sites were investigated as possible ORR active sites: boron heteroatom itself (gB-G-B) and the carbon next to boron (gB-G-C), in which the free energy of intermediate OOH* adsorption on former is 0.50 eV lower than that on the latter. Therefore, gB-G-B is the active site with the reaction intermediates illustrated in Fig. S10b-d.

For OB-G model, four sites were investigated: boron heteroatom itself, the carbon next to the boron atom (C1), the next neighbour carbon on edge (C2-edge), and centre (C2-centre). The first two sites are not identified as active centre due to the inability of O* adsorption on

the boron atom, and inability of OOH*/OH* adsorption. The overall free energy barrier of C2-edge (pathway shown in Fig. S10a) is significantly lower than that on C2-center ($\Delta G_{OOH*}(U^0)$=2.40eV, $\Delta G_{O*}(U^0)$=0.45eV, and $\Delta G_{OH*}(U^0)$=1.69eV, pathway not shown here) and hence it is more active; the reaction intermediates on C2-edge are illustrated in Fig. S10e-g.

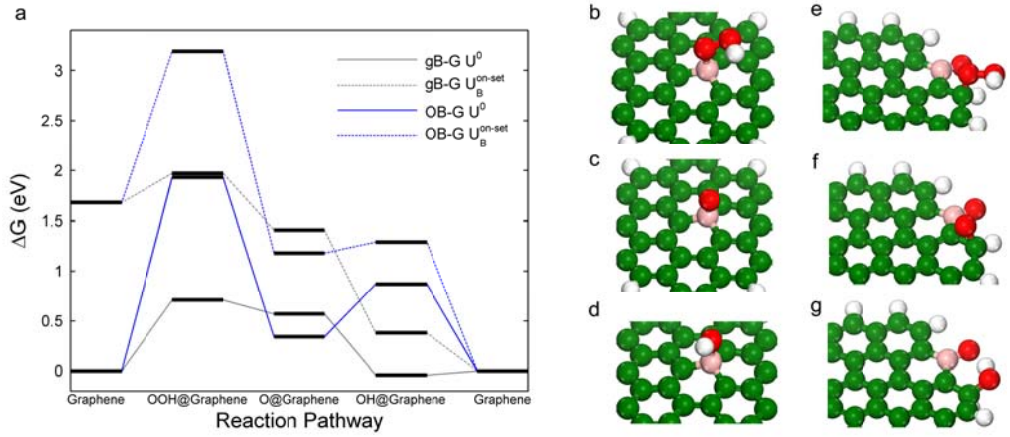

Figure S10 (a) Free energy diagram at U^0 (solid lines) and experimentally observed on-set potential $U_B^{on\text{-}set}$(dash lines) for gB-G (grey) and OB-G (blue). Reaction intermediates on gB-G-B (**b-d**) and OB-G-C2-edge (**e-g**). Green is carbon, red is oxygen, pink is boron, and white is hydrogen.

Nitrogen-Doped Graphene (N-G)

For the three models investigated for nitrogen doped graphene (gN-G, prN-G, and pdN-G), the most active doping pattern is gN-G due to its lowest overall reaction barriers at U^0 (Fig. S11a). The overall reaction barrier on such model is 0.70 eV, and which is reduced to 0.26 eV when at experimentally observed activation electrode potential $U_N^{on\text{-}set}$=0.029 eV.

The active sites for gN-G (Fig. S6d) and prN-G (Fig. S6f) models are all carbons next to graphitic nitrogen atoms, the same as previously reported [1,5,6]; the reaction intermediates are illustrated in Fig. S11b-g. For gN-G model, the OOH* adsorption free energy on the nitrogen heteroatom itself is 1.02 eV, higher than that on the carbon next to the nitrogen and is not considered as an active site for ORR. For prN-G model, OOH and OH cannot form chemisorption on the nitrogen atom, hence it is not considered as active site either. For pdN-

G model (Fig. S6e), the active centre is nitrogen, with reaction intermediates illustrated in Fig. S11h-j. Such behaviour could be attributed to the electron lone pair on the pyridinic nitrogen. Concerning such model, the OOH* adsorption free energy on the carbon next to the pyridinic nitrogen is as high as 2.19 eV, and could not assure an effective O* adsorption.

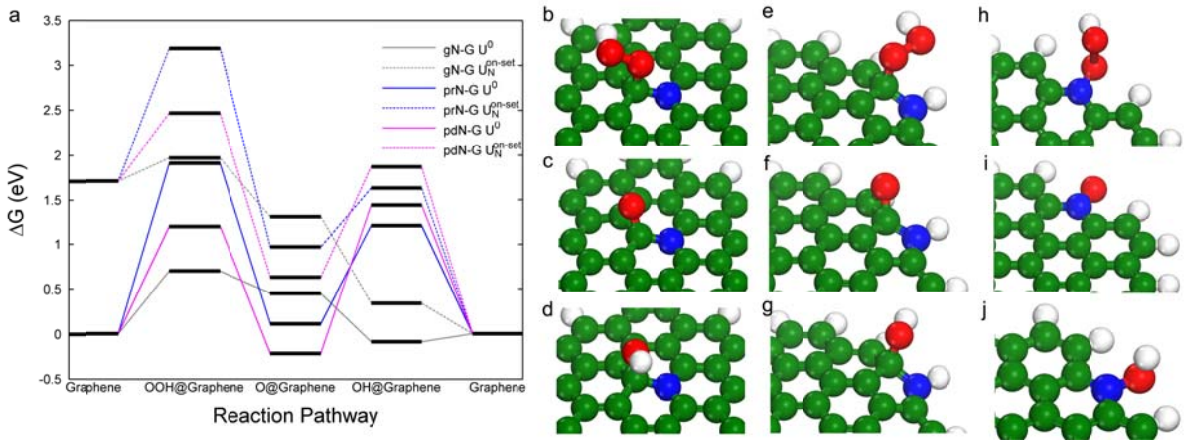

Figure S11 (a) Free energy diagram at U^0 (solid lines) and experimentally observed on-set potential $U_N^{on\text{-}set}$(dash lines) for gN-G (grey), prN-G (blue), and pdN-G (magenta), respectively. Reaction intermediates on gN-G (**b**-**d**), prN-G (**e**-**g**), and pdN-G (**h**-**j**), respectively. Green is carbon, red is oxygen, blue is nitrogen, and white is hydrogen.

Oxygen-Doped Graphene (O-G)

The constitution of experimentally derived O-G is very complicated; here we chose four doping types based on our XPS results and previous theoretical investigations[7]. These four models are pyO-G, C=O-G, epO-G, and C-OH-G as defined in Fig. S6g-j. The most active doping type is pyO-G model (Fig. S6g) with a 0.91 eV overall reaction barrier at U^0, the corresponding active site is carbon next to oxygen (pyO-G-C1) (Fig. S12b-d). Such barrier value is reduced to 0.43 eV at the experimentally observed activation potential $U_{OG}^{on\text{-}set}$= -0.017 V (Fig. S12a). The oxygen itself (pyO-G-O) and the carbon, which is the next neighbour of oxygen (pyO-G-C2) could not bind to oxygen gas, and exhibits a 2.07 eV overall barrier, respectively, hence could not be the active centre.

For C-OH-G model (Fig. S6h), three carbons were investigated: the carbon directly connected to the hydroxyl group (C1), the carbon next to C1, and the edge carbon in the adjacent ring. C1 is considered as the active centre due to the lowest overall energy barrier 1.06 eV (Fig. S12e-g).

For C=O-G model (Fig. S6i), three carbons were investigated: the carbon directly connected to the oxygen (C1), the carbon next to C1 (C2), and the edge carbon in the adjacent ring (C3). C2 is considered as the active centre due to the lowest overall energy barrier 1.15 eV (Fig. S12h-j). On C1, OOH could not form effective bonding while the energy barrier for C3 as active centre is 1.87 eV.

For epO-G model (Fig. S6j), the active carbon atom (carbon-active) is next to the one that directly connects to oxygen (carbon-epoxy). Other carbon atoms that are not directly connected to carbon-epoxy could not facilitate OOH chemisorption; such inactive behaviour could be attributed to the fact that the π bonding on these carbons is not disturbed due to epoxy oxygen bonding. The adsorption configurations of reaction intermediates on carbon-active are illustrated in Fig. S12k-m.

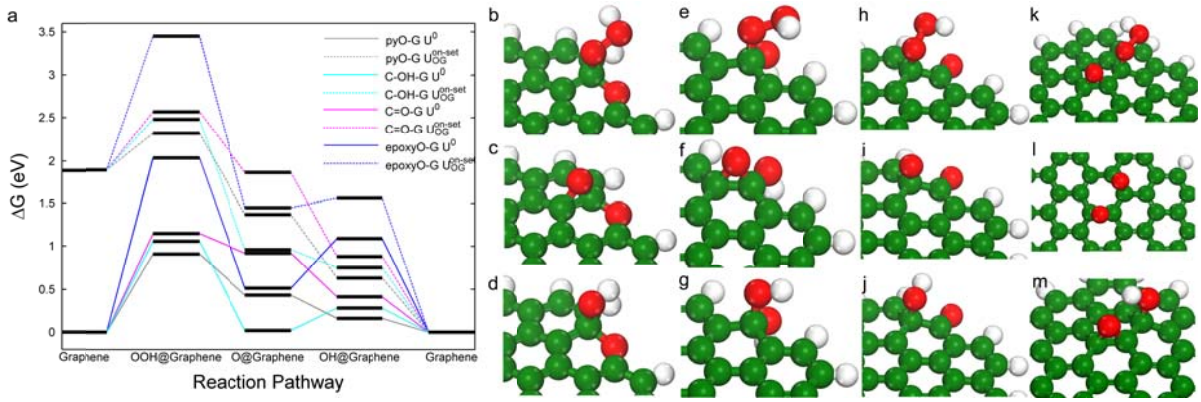

Figure S12 (a) Free energy diagram at U^0 (solid lines) and experimentally observed on-set potential $U_{OG}^{on\text{-}set}$ (dash lines) for pyO-G (grey), C-OH-G (cyan), C=O-G (magenta), and epO-G (blue), respectively. The reaction intermediates on pyO-G (**b**-**d**), C-OH-G (**e**-**g**), C=O-G (**h**-**j**), and epO-G (**k**-**m**) respectively. Green is carbon, red is oxygen, and white is hydrogen.

Phosphorous-Doped Graphene (P-G)

Due to the asymmetry of the cluster model (Fig. S6k), the configurations are shown in Fig. S13b-d for intermediates on the same side with P-O bonding (PG-up), and Fig. S13e-f for intermediates on the different side with P-O bonding (PG-down). These two models exhibit similar overall reaction barrier at U^0, while PG-up model shows a slightly lower value of 0.84 eV, and is considered as active site. Such barrier value is reduced to 0.37 eV at the experimentally observed activation potential $U_{PG}^{on\text{-}set}$= -0.01 V (Fig. S13a).

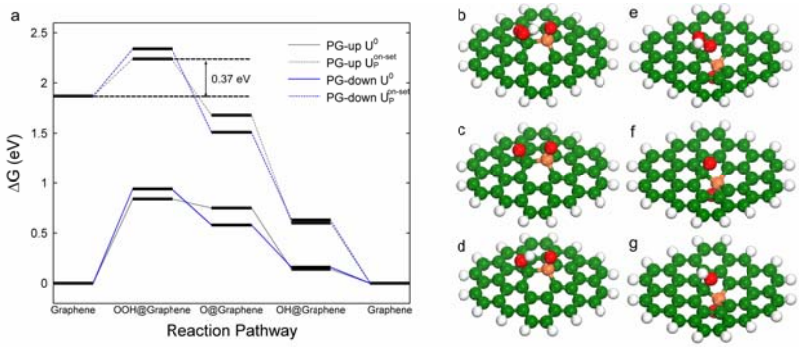

Figure S13 (a) Free energy diagram at U^0 (solid lines) and experimentally observed on-set potential (dashed lines) for PG-up (grey) and PG-down (blue). The reaction intermediates for PG-up (**b**-**d**) and PG-down (**e**-**f**). Green is carbon, red is oxygen, orange is phosphorous, and white is hydrogen.

Sulphur-Doped Graphene (S-G)

For SC6-G model (Figure S6l), several sites were investigated towards its ability for oxygen reduction reaction, which are the doped sulphur atom (S), the carbon next to sulphur (C1), and the carbon which is the second neighbour of doped sulphur (C2). The site that possess the lowest overall barrier at equilibrium potential is C1; while the electrode potential shifts to the experimentally observed activation potential $U_S^{on\text{-}set}$=–0.058 V, the barrier value is reduced from 1.02 eV to 0.51 eV, hence facilitating the oxygen reduction reaction; the intermediates are illustrated in Fig. S14b-d.

For SC5-G model (Fig. S6m), which represents thiophen type S doping, three sites were investigated toward their ability for oxygen reduction, which are the sulphur site (S), carbon

next to sulphur (C1) and the second neighbour carbon (C2). $\Delta G_{eq(9a)}(U^0)$ for these three sites are 1.15 eV for S, 1.97 eV for C1, and 1.25 eV for C2, respectively; however OOH could not chemisorb on the sulphur atom hence it is not considered as active. Hence C2 is considered to be the most active among the three; the intermediate states on C2 are illustrated in Fig. S14e-f.

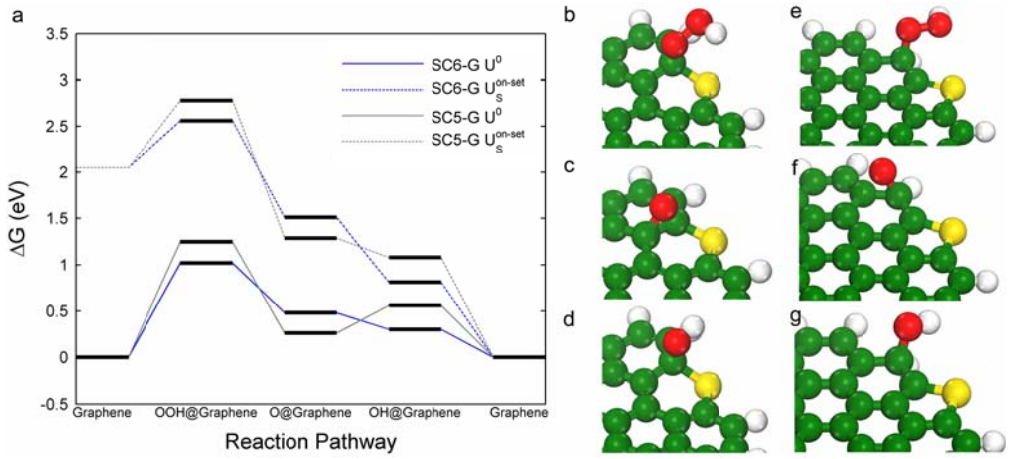

Figure S14 (a) Free energy diagram at U^0 (solid lines) and experimentally observed on-set potential $U_S^{on\text{-}set}$ (dash lines) for SC6-G (blue), SC5-G (grey), respectively. The atomic configurations to the right are reaction intermediates on SC6-G (**b**-**d**), and SC5-G (**e**-**g**). Green is carbon, red is oxygen, yellow is sulphur, and white is hydrogen.

2.5 Adsorption of Intermediates

Table S3 Adsorption free energy of oxygen-containing intermediates for ORR. The molecular orbital analysis and the charge/spin density on the investigated atoms are obtained from NBO analysis (The initial configuration for OOH, O, and OH adsorption on each cluster was obtained by locating corresponding adsorbates 1~1.5Å above the investigated active sites).

Model and Investigated Sites[a]	ΔG_{OOH*}[b] (eV)	ΔG_{O*}[c] (eV)	ΔG_{OH*} (eV)	Charge (e)	Spin	Highest Valance Orbital Energy of the Graphene Cluster (eV)	Lowest Valance by the Active Centre (eV)	E_{diff} (eV)
G-M-C	2.50	1.81	2.04	0	0	0.0894	-0.09862	-0.18802
G-E-C	2.48	1.05	0.90	-0.188	0	0.0894	-0.14854	-0.23794
gB-G-B	2.07	1.48	0.42	0.602	0.078	0.23317	0.03822	-0.19495
gB-G-C	2.58	0.71	0.99	-0.275	0.148	0.23317	-0.12516	-0.35833
OB-G-C2-edge	3.30	1.25	1.32	-0.219	0	0.24355	-0.16469	-0.40824
OB-G-C2-centre	3.77	1.36	2.14	-0.042	0	0.24355	-0.11914	-0.36269
gN-G-C	2.06	1.36	0.37	0.204	0.155	0.09428	-0.14412	-0.24315
pdN-G-C	3.56	2.36	1.94	0.205	0	0.1001	-0.12414	-0.22424

pdN-G-N	2.56	0.69	1.90	-0.472	0	0.1001	-0.49957	-0.59967
prN-G-C	3.28	1.02	1.66	0.176	0	0.1613	-0.12668	-0.28798
pyO-G-C1	2.27	1.34	0.61	0.346	0.041	0.09861	-0.14900	-0.24761
pyO-G-C2	3.44	1.33	1.76	-0.073	-0.025	0.09861	-0.11859	-0.2172
C-OH-G-C1	2.43	0.93	0.74	-0.212	0	0.1484	-0.13722	-0.28562
C-OH-G-C2	3.48	0.93	1.93	-0.111	0	0.1484	-0.12527	-0.27367
C-OH-G-C3	2.81	0.43	1.24	0.386	0	0.1484	-0.16095	-0.30935
C=O-G-C2	2.51	1.83	0.87	-0.100	0.165	0.10579	-0.14795	-0.25374
C=O-G-C3	3.23	0.71	1.69	-0.196	-0.059	0.10579	-0.16939	-0.27518
epO-G	3.40	1.42	1.55	-0.014	0	0.09719	-0.11017	-0.20736
P-G	2.20	1.66	0.59	-0.402	0.216	0.09635	-0.20627	-0.30262
S-G-C1	2.39	1.10	0.75	-0.185	0.053	0.09841	-0.21656	-0.31497
S-G-S	2.76	0.68	1.29	0.437	0.107	0.09841	-0.26129	-0.81591
S-G-C2	3.13	1.02	1.69	-0.250	-0.078	0.09841	-0.17329	-0.2717
SC5-G-S	2.52	0.91	1.94	0.402	0	0.10036	-0.72742	-0.82778
SC5-G-C1	3.34	1.09	1.72	-0.178	0	0.10036	-0.20358	-0.30394
SC5-G-C2	2.61	1.17	1.02	-0.222	0	0.10036	-0.17249	-0.27285

[a] *The investigated sites on each model are defined in Section 1.4; some of the investigated sites are not shown in this table due to that they could not induce effective OOH* O* or OH* adsorption.* [b] *red values represent abnormal OOH* adsorption. Configurations could be found in Section 1.3.* [c] *red values represent chemisorption with one bond formation, black represents epoxy type adsorption.*

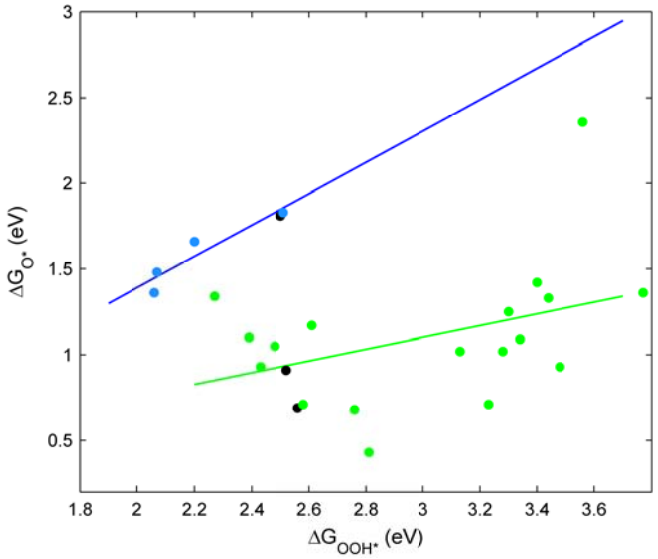

Figure S15 Correlation between ΔG_{O^*} and ΔG_{OOH^*}. Blue dots indicate single bonding, which includes the most active sites on all the investigated graphene clusters – hence the fitted blue line (ΔG_{O^*} = $0.92\Delta G_{OOH^*}$ – 0.44eV) is used to obtain the performance of X-graphene. Green dots indicate epoxy type oxygen adsorption, and the green line follows $\Delta G_{O^*}=0.34\Delta G_{OOH^*}$ – 0.08eV. Black points represent those that could not form chemisorption of OOH* on graphene cluster; hence, they were not considered in line fitting.

2.6 Activation Energies

Table S4 ΔG, half-lives, and completion times of a unimolecular reaction at room temperature, 298 K.

ΔG	Half-Life	97% complete
5 kcal/mol (0.22 eV)	5.7×10^{-5} sec	2.8×10^{-4} sec
10 kcal/mol (0.43 eV)	2.8×10^{-3} sec	1.4×10^{-2} sec
15 kcal/mol (0.65 eV)[a]	0.01 sec	0.05 sec

[a] value taken from reference [8]

References

1. Yu, L., Pan, X. L., Cao, X. M., Hu, P. & Bao, X. H. *J. Catal.* **282**, 183-190 (2011).
2. Yan, H. J., Xu, B., Shi, S. Q. & Ouyang, C. Y. *J. Appl. Phys.* **112**, 104316 (2012).
3. Bard, A. J.; Faulkner, L. R. *Electrochemical Methods: Fundamentals and Applications*; Wiley, 2000.
4. Yuan, W. J. *et al. Sci. Rep-Uk* **3**, 2248 (2013).
5. Zheng, Y., Jiao, Y., Ge, L., Jaroniec, M. & Qiao, S. Z. *Angew. Chem. Int. Edit.* **52**, 3110-3116 (2013).
6. Zhang, L. P. & Xia, Z. H. *J. Phys. Chem. C* **115**, 11170-11176 (2011).
7. Bagri, A. *et al. Nat. Chem.* **2**, 581-587 (2010).
8. Scudder, P. H. *Electron Flow in Organic Chemistry: A Decision-Based Guide to Organic Mechanisms*. 2nd edn, (John Wiley & Sons, 2012).